



HAL
open science

CHARACTERISING DISLOCATION STRUCTURE EVOLUTION DURING CYCLIC DEFORMATION USING ELECTRON CHANNELLING CONTRAST IMAGING

Jaoued Ahmed, Steve G Roberts, Angus Wilkinson

► **To cite this version:**

Jaoued Ahmed, Steve G Roberts, Angus Wilkinson. CHARACTERISING DISLOCATION STRUCTURE EVOLUTION DURING CYCLIC DEFORMATION USING ELECTRON CHANNELLING CONTRAST IMAGING. Philosophical Magazine, 2006, 86 (29-31), pp.4965-4981. 10.1080/14786430600710941 . hal-00513697

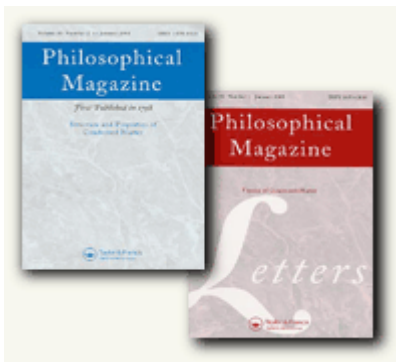
HAL Id: hal-00513697

<https://hal.science/hal-00513697>

Submitted on 1 Sep 2010

HAL is a multi-disciplinary open access archive for the deposit and dissemination of scientific research documents, whether they are published or not. The documents may come from teaching and research institutions in France or abroad, or from public or private research centers.

L'archive ouverte pluridisciplinaire **HAL**, est destinée au dépôt et à la diffusion de documents scientifiques de niveau recherche, publiés ou non, émanant des établissements d'enseignement et de recherche français ou étrangers, des laboratoires publics ou privés.



**CHARACTERISING DISLOCATION STRUCTURE EVOLUTION
DURING CYCLIC DEFORMATION USING ELECTRON
CHANNELLING CONTRAST IMAGING**

Journal:	<i>Philosophical Magazine & Philosophical Magazine Letters</i>
Manuscript ID:	TPHM-05-Nov-0531.R1
Journal Selection:	Philosophical Magazine
Date Submitted by the Author:	19-Feb-2006
Complete List of Authors:	Ahmed, Jaoued; University of Oxford, University of Oxford, Department of Materials Roberts, Steve; University of Oxford, Materials Science Wilkinson, Angus; University of Oxford, Department of Materials
Keywords:	electron channelling, cyclic deformation, fatigue, SEM
Keywords (user supplied):	ECCI



CHARACTERISING DISLOCATION STRUCTURE EVOLUTION DURING CYCLIC DEFORMATION USING ELECTRON CHANNELLING CONTRAST IMAGING

Jaoued Ahmed, Steve G Roberts, and Angus J Wilkinson[†]

Department of Materials, University Of Oxford
Parks Road, Oxford, OX1 3PH, UK

[†]corresponding author

tel: 01865 273792

email: angus.wilkinson@materials.ox.ac.uk

ABSTRACT

This paper briefly reviews development of the electron channelling contrast imaging (ECCI) technique, which uses diffraction contrast to reveal dislocation structures underlying the surface of bulk samples imaged in the scanning electron microscope. In particular the application of ECCI to the study of evolution of dislocation structures during cyclic deformation of single crystal copper samples will be described. Quantitative measurements of the vein width, separation and volume fraction within the matrix phase were made and these parameters showed rapid changes during the initial cyclic hardening of the sample, with smaller variations continuing after stress saturation. The volume fraction of persistent slip bands (PSBs) increased continuously with cycling beyond stress saturation. Measurements of PSB widths and spacings indicated that new PSBs tend to form near existing PSBs. The ECCI technique revealed PSBs of finite length with tapered ends. Stress concentrations occurring ahead of the tapered PSBs may be the cause of preferential nucleation of new PSBs close to existing ones.

1 INTRODUCTION

The electron channelling contrast imaging (ECCI) technique was first suggested as a means of imaging and characterising near surface dislocations in bulk samples by Booker, Shaw, Whelan and Hirsch [1]. The electron-optical conditions required to image dislocations using ECCI was first estimated by Booker [2] who realised that the local tilting of lattice planes near a dislocation was of the order of 10^{-3} rad at 30 nm from the core which makes it necessary to keep both the beam divergence and the probe diameter small. Since the contrast is also small it was clear that a high brightness electron source would be needed to achieve an acceptable signal to noise ratio. More detailed dynamical diffraction calculations by Clarke and Howie [3] and Spencer, Humphreys and Hirsch [4] confirmed this point.

Early experimental efforts to image dislocations using ECCI were hampered by the lack of good field emission guns and thus were of limited success due to poor signal to noise ratio. Morin *et al* [5] were the first to publish clear images of individual dislocations in Si using ECCI in a dedicated SEM with a field emission gun and a retarding field energy filtered back scattered electron detector. Since then several other groups have imaged individual dislocations without the need for the energy filtered BSE detector (eg Czernuszka *et al* [6], Wilkinson and Hirsch [7], and Simkin and Crimp [8]). A more detailed review of the development of ECCI can be found in Wilkinson and Hirsch [9].

Over the past decade there has been considerable interest in applying the ECCI to studies of dislocation patterning and other problems in cyclic deformation and fatigue. One of the main reasons for this is that the technique allows dislocation structures to be imaged in bulk specimens. This offers several significant advantages over TEM methods: (a) it allows the study of dislocation sub-structure to be undertaken in the same specimens at many different points through their fatigue

1
2
3 life, (b) it allows a large area of specimen to be examined, and (c) it allows dislocation structures to
4
5 be directly linked to intrusions, extrusions and cracks that form at the sample surface.
6
7

8
9 In these studies there is no attempt to image individual dislocation lines and as a result the rather
10
11 stringent constraints on the electron-optics can be relaxed making the technique much easier to use.
12

13
14 In particular the constraint on beam diameter can be significantly relaxed so that groups of
15
16 dislocations can be imaged without the need for a field emission gun SEM.
17

18
19 Dudarev, Ahmed, Hirsch and Wilkinson [10] have made a careful study of the contrast generated by
20
21 dislocation walls and veins present in fatigued metals and found that for all useful diffraction
22
23 conditions the highly dislocated regions appeared bright (i.e. higher yield of back scattered
24
25 electrons) compared to the low dislocation density channels between them. The contrast is largest
26
27 when the selected diffraction planes have \mathbf{g} parallel to the primary Burgers vector \mathbf{b} , and at a small
28
29 positive deviation from the exact Bragg condition (i.e. just outside the channelling band edge). The
30
31 bright nature of the dislocation walls and veins was explained within the dynamical diffraction
32
33 theory by the decohesion caused by the rapid fluctuations in the displacement field generated by the
34
35 high dislocation dipole density which occur on a length scale that is significantly shorter than the
36
37 extinction distance.
38
39
40
41

42
43 The ECCI technique has been used to study dislocation patterning in single crystals of copper
44
45 fatigued under stress control by Ahmed, Wilkinson & Roberts [11], and Melisova, Weiss and
46
47 Stickler [12] and under strain control by Li, Hu and Wang [13] and Ahmed, Wilkinson & Roberts
48
49 [14] for single slip, and by Gong, Wang, Chen and Wang [15] for multiple slip. Schwab *et al* [16]
50
51 have made similar studies in Ni single crystals deformed under strain control in single slip. Zhang
52
53 & Wang [17] have used ECCI to examine the effects of grain boundaries on the dislocation
54
55 patterning in cyclically deformed copper polycrystals. The ECCI technique has been used by Chen
56
57
58
59
60 *et al* [18] to investigate dislocation structures ahead of long fatigue cracks in polycrystalline copper,

1
2
3 while recent work by Ahmed, Wilkinson & Roberts [19] shows ECCI images of dislocation
4 structures associated with relatively short, naturally initiated stage I and stage II cracks in single
5 crystal copper. The technique has also been applied to fatigue of engineering materials: e.g. single
6 crystal superalloy by Wilkinson, Henderson & Martin [20], and polycrystalline steels by Davidson
7 & Langford [21], and by Zauter *et al* [22].

8
9
10
11
12
13
14
15
16 Cyclic deformation of cubic close-packed metals (in particular single crystals) generally exhibits an
17 initial period of cyclic hardening, followed by a period of quasi-steady state deformation,
18 'saturation', where the peak stress remains constant with further cycling (see the review by Basinski
19 & Basinski [23]). This saturation régime often takes up a large fraction of the sample life before
20 fatigue failure. Generally for single crystals the peak stress within the saturation régime (τ_{sat})
21 increases with applied plastic strain amplitude (γ_{pl}) up to approximately 10^{-4} and then remains
22 virtually constant in the low strain amplitude region from 10^{-4} to 10^{-2} , before increasing again at
23 higher strain amplitudes [24]. The plateau in the saturation stress – strain amplitude curve is most
24 marked for single slip conditions, and can be reduced or even absent for some multiple slip
25 configurations, as shown by Li, Wang, and Li [25].

26
27
28
29
30
31
32
33
34
35
36
37
38
39
40
41
42
43
44
45
46
47
48
49
50
51
52
53
54
55
56
57
58
59
60
In the plateau region, saturation of the peak stress approximately coincides with the nucleation and
growth of persistent slip bands (PSBs), in which the plastic strain is highly localised. However,
analysis of hysteresis loop shapes by Mughrabi [24] suggests that PSB nucleation may occur before
stress saturation as plastic strain amplitude is increased within the plateau regime. Scanning
electron microscopy has been used in conjunction with the 'sharp corner polishing' method to study
the PSB profiles, which are found to vary somewhat with deformation temperature [23]. The
nucleation of short cracks from intrusions and PSBs has also been investigated using such methods
by Hunsche and Neumann [26], and by Ma and Laird [27]. Transmission electron microscopy
(TEM) has been used to reveal the striking 'ladder' structure of the dislocation configuration within

1
2
3 the PSBs which is markedly different to the dislocation veins (or loop patches) found in the
4 surrounding matrix material (see for example work by Mughrabi, Ackermann, and Hertz [28]).
5
6

7
8 In this paper, we study copper single crystals fatigued under plastic strain control and use the ECCI
9 technique to (i) follow changes in the matrix vein structure both during hardening and after
10 saturation, (ii) examine the initial stages of PSB formation at saturation and (iii) follow the increase
11 in PSB volume fraction and changes in PSB dislocation structures with continued cycling beyond
12 saturation. Wherever possible quantitative parameterisation of the dislocation structures has been
13 obtained from the ECCI images.
14
15
16
17
18
19
20
21
22
23
24
25

26 **2 EXPERIMENTAL PROCEDURES**

27 **2.1 Materials & Sample Preparation**

28 [541] oriented rods were kindly provided by Prof. Z S Basinski. These had been grown from seed
29 from 99.999% Arsaco copper in prepurified graphite moulds under a vacuum as described by
30 Basinski and Basinski [29]. For the [541] loading axis the primary slip system is $\frac{a}{2}[101](\bar{1}\bar{1}\bar{1})$. 60
31 mm long samples with 4 mm x 4 mm square cross-section were prepared with one pair of faces (the
32 ‘cross glide faces’) parallel to $(1\bar{1}\bar{1})$ and the remaining ‘side faces’ parallel to $(1\bar{2}3)$. The cross
33 glide faces contain the primary Burgers vector and remain flat during fatigue while the side faces
34 roughen as the PSBs are formed. The sharp corner preparation technique described by Basinski and
35 Basinski [30] was used so that the profiles of intrusions, extrusions and cracks could be clearly
36 observed, so that they could be directly related to dislocation structures using ECCI, as has been
37 reported by Ahmed *et al* [19].
38
39
40
41
42
43
44
45
46
47
48
49
50
51
52
53
54
55

56 **2.2 Mechanical Testing**

57 The specimens oriented with [541] along the load axis were fatigued in push-pull at room
58 temperature, in laboratory air, at constant plastic shear strain amplitudes γ_p of 10^{-3} and 2×10^{-3}
59
60

1
2
3 measured using a clip-on extensometer (10 mm gauge length) fixed on a side face. An ESH servo-
4
5 hydraulic testing machine fitted with a 10kN load cell with a range down to 1kN was used, with
6
7 specimen alignment ensured by use of a Wood's metal grip system designed and built specifically
8
9 for this work. Parameters such as total strain, plastic strain, load and number of cycles were
10
11 recorded during testing. Testing was at 1 Hz with a sine waveform.
12
13
14

15 16 **2.3 Electron Channelling Contrast Imaging**

17 The SEM studies using ECCI and secondary electron (SE) modes were carried out in a JEOL
18
19 JSM6300 SEM with a LaB₆ filament. The SEM stage allowed continuous rotation through 360°
20
21 about an axis perpendicular to the samples' surface and tilting about an orthogonal axis within the
22
23 samples' surface plane. The sample was tilted/rotated while viewing the electron channelling
24
25 pattern (ECP) so as to achieve the desired diffraction conditions. The conditions used to observe
26
27 dislocation substructures from bulk samples of copper single crystals were as follows: incident
28
29 beam energy of 30 keV, probe current of 2nA, estimated probe divergence of 3 mrad (half angle
30
31 subtended by a 50 μm aperture diameter at 8 mm working distance), and an estimate probe diameter
32
33 of 65 nm. ECCI experiments in this work were carried out mainly using the diffraction conditions
34
35 such that $\mathbf{g}\cdot\mathbf{b}=2$ along the (202) band near the $[1\bar{1}\bar{1}]$ zone axes of the cross glide face; the
36
37 observations were thus made at close to normal incidence. From time to time other diffraction
38
39 conditions were used and these are specified and shown in ECPs accompanying the ECCI
40
41 micrographs. The dark outer edge of the (202) band ($w>0$) was used to image dislocations: $w = \mathbf{s}|\xi_g$
42
43 represents the deviation parameter as defined in Hirsch *et al.* [31] where ξ_g is the extinction
44
45 distance. The detector used to image the flat cross glide face was the standard diode type annular
46
47 BSE detector mounted below the pole piece in the SEM. Digital image acquisition was carried out
48
49 using a PC system with an 8 bit frame grabber. In order to reduce noise in the signal, images were
50
51 averaged over several frames with a typical image acquired over a period of 30 to 60 seconds.
52
53
54
55
56
57
58
59
60

3 RESULTS

3.1 Mechanical Properties

The cyclic hardening curves obtained at constant plastic strain amplitudes of 10^{-3} and 2×10^{-3} were similar to those previously obtained for the same specimen orientation by Basinski *et al.* (1992). Rapid hardening occurs during the first few thousands of cycles before the peak stress reaches a maximum value (after ~5000 cycles) of ~28 MPa. During saturation, the peak stress is constant to a first approximation though a slight decrease can be seen from the maximum value. This is in good agreement with values of the saturation stress in the literature [23] which vary between 27MPa-32MPa depending on testing parameters such as the strain rate, the exact testing temperature etc..

3.2 Dislocations Structures up to Stress Saturation

A specimen cycled at a constant plastic strain amplitude of 2×10^{-3} was examined using ECCI at different numbers of cycles (N) before the stress amplitude reached the saturation value of 28 MPa. Figure 1 shows the matrix vein structure in bright contrast at (a) 50 and (b) 2000 cycles. The dark regions represent the low dislocation density areas ('channels') separating the primary walls. After 50 cycles (Fig. 1a), the matrix dislocation structure already consists of dislocation walls, however these features appeared to be of lower contrast than structures seen further into the fatigue life. With further cycling to N = 2000 cycles (Fig. 1b), the walls thicken along the primary Burgers vector but reduce in height perpendicular to the primary Burgers vector.

With further cycling, the shear stress amplitude approaches the saturation stress and the matrix vein structure undergoes some local changes. Whereas most of the dislocation structure still consists of large thick veins separated by low dislocation density channels, ECCI reveals the presence of some thin dislocation walls embedded within the vein structure. This is illustrated in Figure 2 where the beginning of the formation of PSBs can be observed as the stress reaches 25 MPa after 2500 cycles.

1
2
3
4
5
6
7
8
9
10
11
12
13
14
15
16
17
18
19
20
21
22
23
24
25
26
27
28
29
30
31
32
33
34
35
36
37
38
39
40
41
42
43
44
45
46
47
48
49
50
51
52
53
54
55
56
57
58
59
60

White arrows indicate the formation of thin dislocation walls from the matrix veins; these walls are different from the surrounding structure.

After further fatigue to 5000 cycles the peak stress reaches the saturation value of 28 MPa and at this point ECCI reveals the formation of PSBs from the matrix structure (Figure 3). The dislocation walls characterising these “young” PSBs are inclined, making an angle of about 60° with the primary slip direction, while later in the fatigue life the walls tend to align perpendicular to the slip direction.

Although the resolution attainable by ECCI is significantly lower than that in TEM, it is possible to identify the nucleation of PSB walls from the matrix vein structure. The black arrows in Figure 3 indicate regions where the partial collapse of the loop patches (veins) has taken place and narrow PSB walls connect the two remaining parts of the veins. There appears to be some tendency for the PSB walls to be associated with the edge of the veins from which they have formed.

3.3 Dislocations Structures After Stress Saturation

Figure 4 shows an ECCI micrograph of a bulk sample fatigued well into stress saturation (40000 cycles at a strain amplitude of 2×10^{-3}). The micrograph is at relatively low magnification and demonstrates the utility of ECCI in examining larger area than would be accessible using TEM. Several well established PSBs are seen within the matrix structure and run across the entire field of view. A considerable range of PSB widths is evident in the image, and in the wider PSBs it is evident that the dislocation walls are approximately perpendicular to the slip direction, and the walls are fairly uniformly spaced at $\sim 1.4 \mu\text{m}$ apart.

Several of the thinner PSB (arrowed) do not cross the whole field of view in figure 4. The width of these PSBs is seen to decrease steadily as they taper toward a point in this low magnification image. Figure 5 gives a further example in a sample fatigued for 180000 cycles. There is little evidence for perturbation of the dislocation veins directly ahead of the tip of a PSB. For example in figure 5 the

1
2
3 PSB passes through vein A where 2 small PSB walls can be seen at the vein edges while the next
4
5
6 vein B shows little difference from others within the micrograph. Such ECCI observations made on
7
8
9 several specimens make it clear that PSBs are not always continuous across the entire width of the
10
11 single crystal specimen.

12
13 In the late saturation regime (fig. 6) locally misoriented regions are evident in the ECCI images as
14
15 zones of bright or dark contrast which tend to be elongated along the primary Burgers vector and
16
17 can be several tens of micrometers long. Typically the contrast is relatively constant throughout
18
19 each zone but changes abruptly at its edge, where the change in orientation is localised. Within a
20
21 given misoriented zone dislocation walls can be seen across which there is no change in contrast,
22
23 indicating no change in misorientation.
24
25
26

27 28 **3.4 Evolution of Matrix Veins**

29
30 ECCI was used in a quantitative analysis of the dislocation substructures generated during cyclic
31
32 deformation. The evolution of matrix vein structure was characterised using the following
33
34 parameters: V - the volume fraction of the veins within the matrix regions, W - the average width of
35
36 the dislocation veins (measured along the primary Burgers vector), and D - the width of channels
37
38 between the veins (again measured along the primary Burgers vector). W and D are shown on the
39
40 schematic diagram in figure 7.
41
42

43
44 These parameters were determined from the digitally recorded ECCI micrographs of matrix regions
45
46 in specimens fatigued to different stages of the fatigue life before and after PSB formation. A
47
48 simple thresholding algorithm was used to distinguish between veins and channels and so produce
49
50 binary images from which V , W and D were determined. Figure 8 shows the variation of these
51
52 parameters with the number of fatigue cycles applied. The vein volume fraction V increases
53
54 significantly in the rapid hardening stage from $N=50$ to $N=5000$. After 5000 cycles the stress has
55
56 saturated and the vein volume fraction remains constant over the next several tens of thousands of
57
58 cycles. As more cycles are applied the average matrix channel width D decreases, while the average
59
60

1
2
3 vein width W increases. The most rapid changes again occur during the period of cyclic hardening,
4
5 however, small but significant reduction in the channel width continues after the first PSBs begin to
6
7 form (~ 2000 cycles) and after the stress saturates (~ 5000 cycles).
8
9

10 11 **3.5 Evolution of Persistent Slip Bands**

12 Quantitative measurements were also made of parameters describing the PSB evolution within the
13 stress saturation régime. The widths of PSBs and matrix regions were measured perpendicular to
14 the slip direction (see figure 7) on ECCI micrographs obtained from the cross glide face of the
15 specimen after different amounts of cyclic deformation. From such measurements the PSB volume
16 fraction (f) was also determined. The measurements were made at three different points through the
17 fatigue life, from approximately the same region of one sample fatigued at a strain amplitude of
18 2×10^{-3} . A similar set of measurements were made from a second sample fatigued at a strain
19 amplitude of 10^{-3} .
20
21

22 The variation of PSB volume fraction with cumulative strain (equal to the strain amplitude
23 multiplied by $4N$) is shown in figure 9. The formation of PSBs from the matrix structure is most
24 rapid in the period when the stress starts to saturate, however the continuous increase in f shows that
25 new PSB material is formed throughout the fatigue life. These results are comparable to those
26 obtained by Basinski *et al.* [32] which are also shown in figure 9. The slightly higher PSB volume
27 fractions reported by Basinski *et al* [32] may be due to either their higher strain amplitude or the fact
28 that f was determined in their study from the roughening of the 'side face' rather than, as here,
29 directly from the dislocation structure underlying the surface.
30
31

32 Figure 10 shows how the distributions of PSB widths and matrix widths evolve during the stress
33 saturation régime. Misoriented regions such as shown in figure 6 were not included in this analysis.
34
35 Soon after saturation ($N = 5\ 000$) the majority of PSBs formed have a width below $2\ \mu\text{m}$; only ~ 10
36
37 % possess widths in the range $2\text{-}3\ \mu\text{m}$, and no PSBs with a width greater than $5\ \mu\text{m}$ were observed.
38
39
40
41
42
43
44
45
46
47
48
49
50
51
52
53
54
55
56
57
58
59
60

1
2
3 The spacing between the PSBs (i.e. matrix width) ranges from 1 μm to 30 μm with ~55% in the 5-
4
5
6 15 μm range near the average spacing of ~10 μm .
7

8
9 With further cycling (N= 23400), PSBs with a greater width (>5 μm) are observed and after 40000
10
11 cycles the maximum observed PSB width increases to 20 μm . The frequency of narrow PSBs
12
13 (width <1 μm) range initially drops during the period N= 5000 to 23400 cycles but then
14
15 subsequently increases again with further cycling to 40000 cycles. This suggests that while PSBs
16
17 with a small width have merged together to create new larger PSBs (macro-PSBs), new thin PSBs
18
19 with widths less than 1 μm are also formed.
20
21

22
23 Although both the mean and most common PSB spacing (matrix width) decreases as N increases
24
25 from 5000 to 40000 cycles, it is noticeable that the wider (20-30 μm) matrix regions actually become
26
27 more frequent. This seems to suggest that new PSBs do not form in the centre of large matrix
28
29 regions but instead are preferentially nucleated close to pre-existing PSBs.
30
31
32
33
34
35

36 **4. DISCUSSION**

37 **4.1 Matrix activity**

38
39 The present ECCI observations of the matrix vein structure evolution in bulk samples give
40
41 information that has previously only been attainable through TEM studies involving destructive thin
42
43 foil preparation. The quantitative characterisation of the matrix structure evolution given in figure 8
44
45 is similar to TEM results of Pedersen and Winter [33] whose study was at a slightly higher strain
46
47 amplitude of 3×10^{-3} and treated only the first 5500 cycles. Both studies show that during the period
48
49 of rapid hardening over the first few thousand cycles there is a significant increase in the volume
50
51 fraction occupied by the dislocation veins. This is accomplished by a thickening of existing loop
52
53 patches and a complementary narrowing of the channels between them.
54
55
56
57
58
59
60

The reduction in the channel width leads to an increase in the Orowan-like stress τ_o required for screw dislocations to glide along the channel. Using the expression from Brown [34] for τ_o

$$\tau_o = \frac{\mu b \ln(W/b)}{2\pi(1-\nu)D} \quad (1)$$

where $\mu=42$ GPa and $\nu=0.44$ are the shear modulus and the Poisson's ratio respectively, we find that τ_o is always less than the experimentally measured peak stress (τ_{max}) both in the initial hardening regime and into the saturation regime. It thus appears that at all stages of the fatigue life screw dislocations are able to glide along the channels between matrix veins until they encounter a second screw dislocation of opposite sign, close enough to form a strong dipole. We can estimate the dipole height h that would just prevent motion of the screw dislocations from:

$$h = \frac{\mu b}{4\pi(\tau_{max} - \tau_o)} \quad (2)$$

This assumes that the Orowan - bowing stress and the dipole passing stress are additive, which Lisiecki and Pedersen [35] indicate may not be correct. Figure 11 shows how the stable screw dipole height, calculated from our data and that from Pedersen and Winter [33] varies with N_f . The dipole height decreases during the initial period of hardening and then reaches a near constant value within the saturation regime. Brown [34] has given similar analysis for the PSB structure for which the channel width $D_{PSB} = 1.4 \mu\text{m}$ is somewhat smaller than the vein spacing in the matrix, while the PSB wall width $W_{PSB} = 0.1 \mu\text{m}$ is considerably narrower than the veins. Interestingly, within the saturation regime, the height of dipoles resisting flow of screw dislocations in the channels between matrix veins is essentially the same as that for the channels between walls in the PSB ladder structure (fig. 11). Brown [34] identifies this as the minimum dipole height for which screw dislocation dipoles in Cu are stable against cross-slip and subsequent mutual annihilation, quoting as support Mughrabi's [36] observation that ~ 50 nm is the minimum height of screw dipoles in neutron-pinned TEM foils of fatigued copper. It seems that the formation of stable screw dipoles

1
2
3 within channels between matrix veins occurs over the initial few thousand cycles and contributes to
4
5
6 hardening, but as stress saturation is reached these dipoles are unstable against either the applied
7
8 shear stress (wide dipoles) or against cross-slip (narrow dipoles). It is important to note then that
9
10 although the vein volume fraction remains reasonably constant after the initial period of hardening it
11
12 is likely that there is still dislocation activity in the matrix channels throughout the stress saturation
13
14 regime.
15
16

17
18 Other researchers including Feltner [37], and Kuhlmann-Wilsdorf [38] have instead proposed that
19
20 the matrix straining occurs by the 'flip-flopping' of edge dislocation dipoles within the matrix veins.
21
22 However, the weak beam TEM analysis of Antonopoulos, Brown and Winter [39] found no
23
24 evidence for a preponderance of dipoles in configurations corresponding to the last applied sense of
25
26 shearing and so do not support this mechanism.
27
28

30 **4.2 Initial Nucleation of Persistent Slip Bands**

31
32 At stress saturation a large fraction of the imposed plastic strain becomes localised in the PSBs. As
33
34 the matrix hardens PSBs nucleate within the vein structure by the collapse of matrix veins. The
35
36 vein structure has been studied by Winter [40], Kuhlmann-Wilsdorf and Laird [41], and Jin [42]
37
38 who each concluded that dislocation arrangements at the centre of the veins, accumulated at the
39
40 lower stresses required early in fatigue, tend to be more widely spaced and thus softer than the outer
41
42 shell of dislocations accumulated later on. Nucleation of embryonic PSBs is thus thought to occur
43
44 through the collapse of the vein interiors as the applied stress increases to levels that cannot be
45
46 supported by the softer dislocation structure. Our ECCI observations seem to support this in that
47
48 the walls of PSBs seen in the early stages of formation are generally connected to the outer shell of
49
50 adjacent matrix veins (see figure 3).
51
52
53
54
55

56
57 In the early stages of stress saturation the PSB walls tend to be inclined to the primary Burgers
58
59 vector, as in figure 3, while more established PSB seen after more extensive cycling have walls that
60
are approximately perpendicular to the primary Burgers vector (see figure 4). This may simply be

1
2
3 due to initial alignment of the PSB walls with the existing hard outer shells of the veins from which
4 they formed, which then adjust to a more stable orientation gradually as cycling continues.
5
6
7

8 **4.3 Continuing Persistent Slip Band Formation**

9
10 PSB volume fraction as measured using ECCI on the cross-glide face was found to increase
11 continuously with cycling beyond the stress saturation point. This is in agreement with similar
12 results based on observation of the 'side faces' by Basinski *et al* [32]. The continued conversion of
13 matrix material into new PSB material whilst the peak stress remains essentially unchanged implies
14 that either existing PSBs or the matrix itself is hardening and can no longer accommodate the
15 applied strain. Since the new PSBs must be formed by conversion of the matrix structure it seems
16 unlikely that the matrix is hardening significantly, as this would imply increased resistance to
17 dislocation processes and tends to inhibit conversion to new PSBs. The hardening of 'old' PSBs has
18 been linked to the activation of secondary slip and the formation of misoriented dislocation cell
19 structures such as those seen in figure 6 by Wang and Mughrabi [43]. However, in single crystals
20 such structures are only evident quite late in the fatigue life, or at higher plastic strain amplitudes ,
21 while the observed steady increase in the PSB volume fraction occurs much earlier.
22
23
24
25
26
27
28
29
30
31
32
33
34
35
36
37
38
39

40 The increase in PSB volume fraction could either be through growth of existing PSBs or the
41 nucleation of entirely new PSBs. Our ECCI observations of PSBs of finite length tapering to a
42 point suggest that growth of such a PSB by extension along the slip plane can occur. The larger
43 strain that occurs in the PSB will lead to a stress concentration at the PSB tip which will encourage
44 collapse of matrix veins in the vicinity. The tapered PSB thus grows by destabilising the matrix
45 veins directly ahead of it and propagating forward along the slip plane. The observation that the
46 wider regions of matrix remain present in the samples even though the PSB volume fraction is
47 increasing as deformation continues also suggests that there is some mechanism in operation that
48 causes new PSBs to nucleate close to existing ones. The stress concentration near the tapered tip of
49 PSB may cause collapse of a vein that is slightly displaced from the slip plane on which the existing
50
51
52
53
54
55
56
57
58
59
60

1
2
3 PSB is growing. A new PSB on a near by slip plane can thus be nucleated, which is in accord with
4
5 the observed increase in the frequency of narrow (2-3 μm) matrix regions as cyclic deformation
6
7 continues.
8
9

10 11 12 13 14 **5. CONCLUSIONS**

15 ECCI extends the usefulness of the SEM by allowing crystallographic defects to be revealed in bulk
16 samples. This is particularly useful in the study of cyclic deformation where the evolution of
17 dislocation structures can be followed in the same sample throughout its fatigue life. From this
18 study of copper single crystals fatigued up to and beyond saturation of the shear stress amplitude,
19 the following conclusions can be drawn:
20
21
22
23
24
25
26
27

- 28 1) ECCI can easily image and distinguish matrix vein, PSB ladder, and misoriented cell structures.
29
30 Furthermore quantitative measurement of the dislocation structures can be made.
31
32
- 33 2) Matrix veins increase in width and decrease in separation rapidly during the initial period of
34 cyclic hardening. Throughout stress saturation the matrix remains plastically active since there
35 is sufficient stress to cause motion of screw dislocations in the matrix channels.
36
37
38
39
- 40 3) The earliest PSBs observed indicate formation through the collapse of vein interiors. Newly
41 formed PSBs possess walls that are inclined to the primary slip direction.
42
43
44
- 45 4) The PSB volume fraction increases continuously throughout the fatigue life indicating that older
46 PSBs harden and so contribute less to the overall strain.
47
48
49
50
- 51 5) ECCI revealed PSBs of finite length tapering to a point. The stress concentration ahead of a
52 tapering PSB could help achieve the increase in PSB volume fraction by either growth of the
53 existing PSB along its slip plane, or by nucleation of a new PSB on a nearby parallel slip plane.
54
55
56
57
58
59
60

6. ACKNOWLEDGEMENTS

The authors thank Professor Sir Peter Hirsch and Dr John Martin for useful discussions through the course of this work, and acknowledge the late Professor Z S Basinski for his generous supply of single crystals. The work was supported by the EPSRC. AJW thanks the Royal Society for their support through the University Research Fellowship scheme.

REFERENCES

- [1] Booker G. R. , Shaw A. M. B. , Whelan M. J. and Hirsch P. B. 1967, *Phil. Mag.* **16**, 1185-1191
- [2] Booker G. R. , 1970. in *Modern diffraction and imaging techniques in materials science*, ed. Amelinkx S. , Gevers R. , Remant R. and van Landuyt J. (North Holland, Amsterdam)
- [3] Clarke D. R. and Howie A. , 1971, *Phil. Mag.* **24**, 959-971
- [4] Spencer J. P., Humphreys C. J. and Hirsch P. B. , 1972. *Phil. Mag.* , **26**, 193-213
- [5] Morin P. , Pitaval M. , Besnard D. and Fontaine G. , 1979, *Phil. Mag. A*, **40**, 511-524
- [6] Czernuszka J. T. , Long N. J. , Boyes E. D. and Hirsch P. B. , 1990, *Phil. Mag. Lett.* , **62**, 227-232
- [7] Wilkinson A. J. and Hirsch P. B. , 1995, *Phil. Mag. A*, **72**, 81-103
- [8] Simkin B A and Crimp M A, 1999. *Ultramicroscopy*, **77**, 65-76
- [9] Wilkinson, A. J. and Hirsch P. B., 1997, *Micron*, **28**, 279.
- [10] Dudarev, S. L., Ahmed, J., Hirsch, P. B. and Wilkinson, A. J., 1999, *Acta Cryst.* **A55**, 234.
- [11] Ahmed, J., Wilkinson, A. J. and Roberts, S. G., 1997, *Phil. Mag. Lett.*, **76**, 237.
- [12] Melisova D., Weiss B. and Stickler R., 1997, *Scripta Metallurgica*, **36**, 1061-1066.

-
- 1
2
3
4
5
6 [13] Li, X. W., Hu, Y. M., and Wang, Z. G., 1998, *Material Science & Engineering*, **A248**, 299-303
7
8
9 [14] Ahmed, J., Wilkinson, A. J. and Roberts, S. G., 1999, *J. Microscopy*, **195**, 197-203.
10
11
12 [15] Gong, B., Wang, Z., Chen, D., and Wang, Z. G., 1997, *Scripta Metallurgica*, **37**, 1605-1610.
13
14
15 [16] Schwab A., Bretschneider J., Buque C., Blochwitz C. and Holste C., 1996, *Philosophical*
16
17 *Magazine Letters*, **74**, 449.
18
19 [17] Zhang Z.F. and Wang Z. G., 1998, *Phil. Mag. Lett.*, **78**, 2, 105-113.
20
21
22 [18] Chen, D. L., Melisova, D. Weiss, B. and Stickler, R., 1997, *Fatigue Fract. Eng. Mater. Struct.*,
23
24
25 **20**, 1551.
26
27 [19] Ahmed, J., Wilkinson, A. J. and Roberts, S. G., 2001, *Phil. Mag. A.*, **81**, 1473-1488
28
29
30 [20] Wilkinson A. J., Henderson M. B., and Martin J. W., 1996, *Phil. Mag. Letters*, **74**, 145-151
31
32
33 [21] Davidson, D. L., and Lankford, J., 1981, *Int. J. Fracture*, **17**, 257-275.
34
35
36 [22] Zauter R., Petry F., Bayerlein M., Sommer C., Christ H.-J. and Mughrabi H., 1992, *Phil. Mag.*
37
38 *A*, **66**, 425.
39
40 [23] Basinski, Z. S. and Basinski, S. J., 1992, *Progress in Materials Science*, **36**, 89.
41
42
43 [24] Mughrabi H., 1978, *Materials Science and Engineering*, **33**, 207-223.
44
45
46 [25] Li, X. W., Wang, Z. G., Li, S.X., 1999, *Phil. Mag. Letters*, **79**, 715-719.
47
48
49 [26] Hunsche, A. and Neumann, P, 1986, *Acta Metallurgica*, **34**, 207.
50
51
52 [27] Ma, B.-T. and Laird, C., 1989, *Acta Metall.*, **37**, 325.
53
54 [28] Mughrabi H., Ackermann F. and Herz K., 1979, *Fatigue Mechanisms*, Special Technical
55
56 Report 675, ASTM, Philadelphia, pp. 69-105.
57
58
59 [29] Basinski, Z. S. and Basinski, S. J., 1985, *Acta Metallurgica*, **33**, 1319.
60

- 1
2
3
4
5
6 [30] Basinski, Z. S. and Basinski, S. J. ,1984, *Scripta Metallurgica*, **18**, 851-856.
7
8
9 [31] Hirsch P. B., Howie A., Nicholson R. B., Pashley D. W. and Whelan M. J., 1965, *Electron*
10
11 *Microscopy of Thin Crystals*, (Butterworths, London).
12
13
14 [32] Basinski, Z. S., Pasucal, R., and Basinski, S. J., 1983, *Acta Metallurgica*, **31**, 4, 591-602.
15
16
17 [33] Pedersen, O. B., and Winter, A. T., 1995, *Physica Status Solidi A*, **149**, 281-296.
18
19
20 [34] Brown, L. M., 2000, *Mater. Sci. Eng. A*, **A285**, 35-42.
21
22
23 [35] Lisiecki L. L and Pedersen O. B. 1991, *Acta Mater.*, **39**, 1449-1456
24
25 [36] Mughrabi H., 1979, in *Proc. 5th Int. Conf. Strength of Metals & Alloys*, Eds. Haasen, P.,
26
27 *Gerold, V. & Kostorz G*, (Pergamon Press, Oxford), pp 1615.
28
29
30 [37] Feltner, C. E., 1965, *Philosophical Magazine A*, **12**, 1229-1248.
31
32
33 [38] Kuhlmann-Wilsdorf, D., 1979, *Materials Science and Engineering*, **39**, 231-245
34
35
36 [39] Antonopoulos, J. G., Brown, L. M. and Winter, A. T., 1976, *Phil. Mag.*, **34**, 549.
37
38
39 [40] Winter A. T., 1978, *Philosophical Magazine*, **37**, 457-463.
40
41
42 [41] Kuhlmann-Wilsdorf, D., and Laird, C., 1977, *Materials Science and Engineering*, **27**, 137
43
44 [42] Jin N. Y., 1989, *Acta Metallurgica*, **37**, No7, pp. 2055-2066.
45
46 [43] Wang R, and Mughrabi H, 1984 *Mater. Sci. Engng*, **63**, 147-163
47
48
49
50
51
52
53
54
55
56
57
58
59
60

8. FIGURE CAPTIONS

Figure 1 ECCI micrographs obtained from the cross glide face after cycling at a plastic strain amplitude of 2×10^{-3} for (a) 50 cycles and (b) 2000 cycles. Considerable thickening of the initial matrix walls into matrix veins is clearly evident.

Figure 2: ECCI micrograph obtained from the cross glide face after cycling at a plastic strain amplitude of 2×10^{-3} for 2500 cycles. A few thin dislocation walls (white arrows) can be seen within the matrix vein structure.

Figure 3: ECCI micrograph obtained from the cross glide face after cycling at a plastic strain amplitude of 2×10^{-3} for 5000 cycles. PSBs have now nucleated within the matrix. Note the inclination of the walls forming the PSBs.

Figure 4: ECCI micrograph obtained from the cross glide face after cycling at a plastic strain amplitude of 2×10^{-3} for 40000 cycles. Well-established PSBs span the image and have walls perpendicular to the slip direction. Other thinner PSBs (arrowed) do not span the micrograph.

Figure 5: ECCI micrograph obtained from the cross glide face after cycling at a plastic strain amplitude of 2×10^{-3} for 180000 cycles. The two arrowed PSBs taper to a point and end within the micrograph.

Figure 6: ECCI micrograph obtained from the cross glide face after cycling at a plastic strain amplitude of 10^{-3} for 180000 cycles. Regions at the top and bottom of the micrograph show local misorientations.

Figure 7: Schematic diagram showing the parameters used to describe the matrix and PSB microstructures.

1
2
3
4
5
6
7
8
9
10
11
12
13
14
15
16
17
18
19
20
21
22
23
24
25
26
27
28
29
30
31
32
33
34
35
36
37
38
39
40
41
42
43
44
45
46
47
48
49
50
51
52
53
54
55
56
57
58
59
60

Figure 8: Evolution of vein volume fraction within matrix (V), vein width (W) and channel width D with number of applied fatigue cycles at a plastic shear strain amplitude of 2×10^{-3} .

Figure 9: Increase in PSB volume fraction with cumulative strain.

Figure 10: Histograms showing distributions of PSB widths and matrix region widths measured from ECCI micrographs taken of the cross glide face of a sample after fatigue for differing numbers of cycles at a strain amplitude of 2×10^{-3} .

Figure 11: Decrease in calculated height of screw dipoles within matrix channels that are just stable against separation by applied peak stress.

10 FIGURES

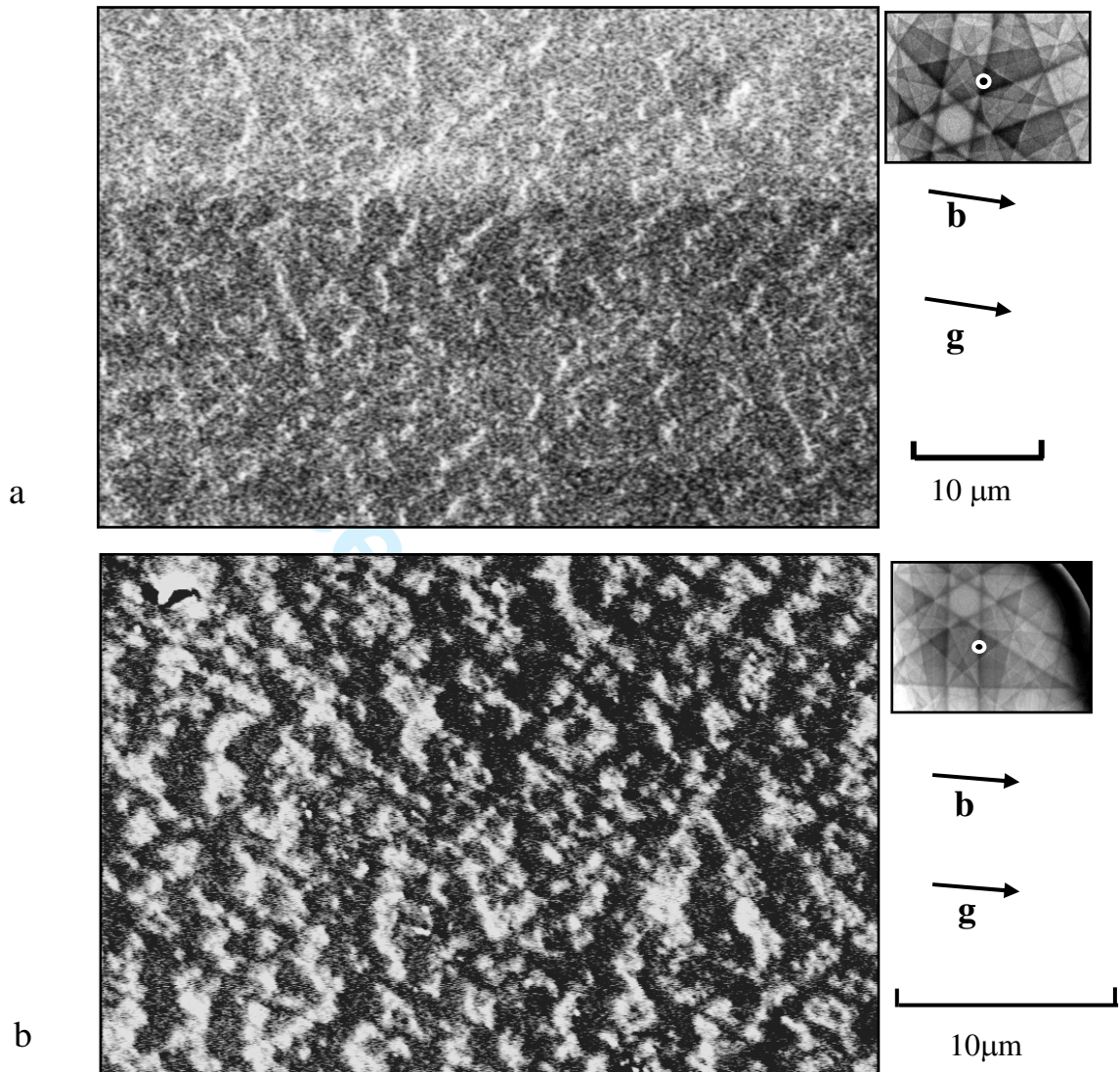


Figure 1: ECCI micrographs obtained from the cross glide face after cycling at a plastic strain amplitude of 2×10^{-3} for (a) 50 cycles and (b) 2000 cycles. Considerable thickening of the initial matrix walls into matrix veins is clearly evident.

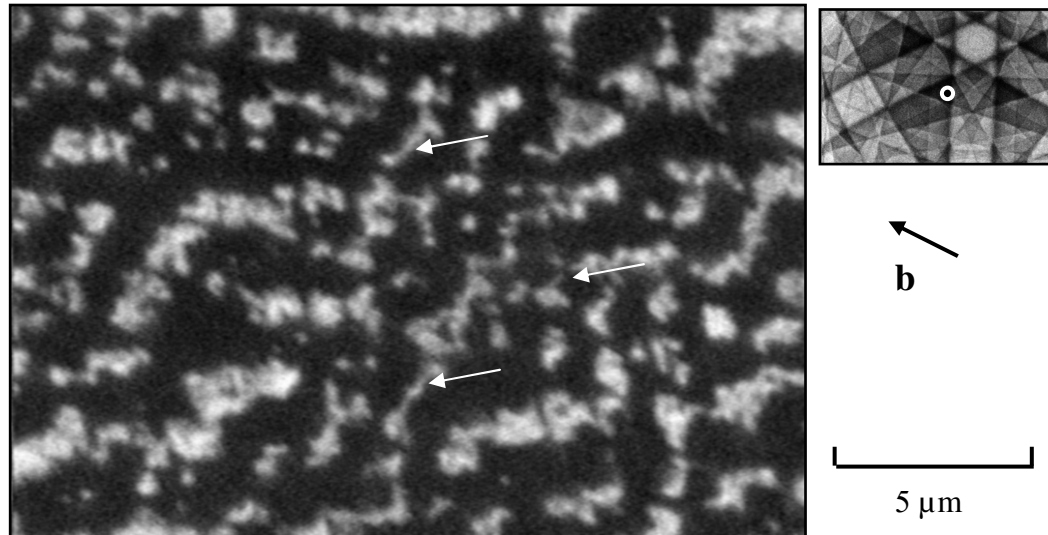


Figure 2: ECCI micrograph obtained from the cross glide face after cycling at a plastic strain amplitude of 2×10^{-3} for 2500 cycles. A few thin dislocation walls (white arrows) can be seen within the matrix vein structure.

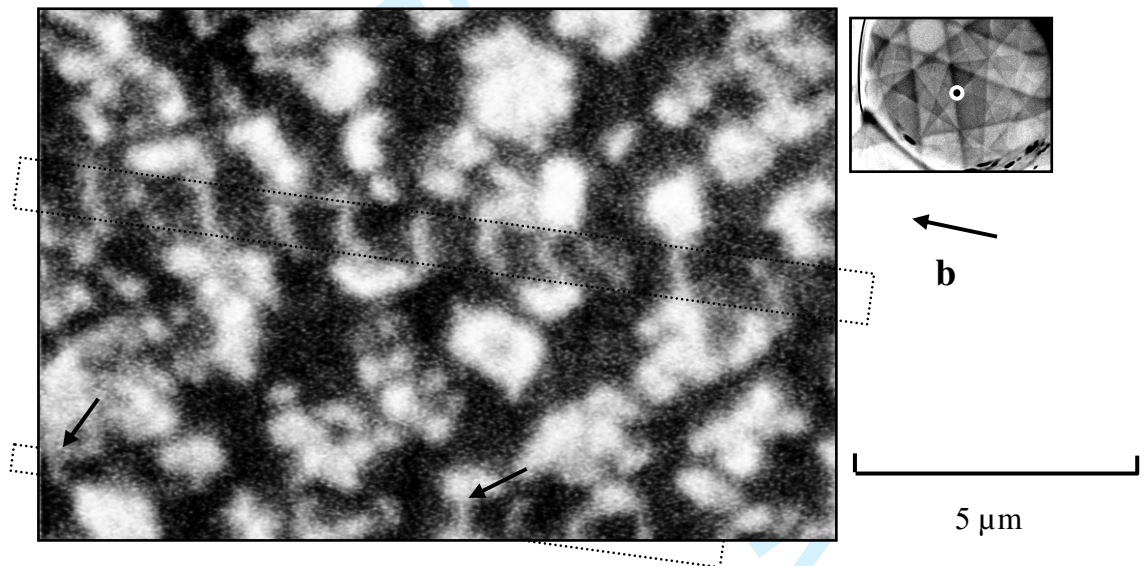
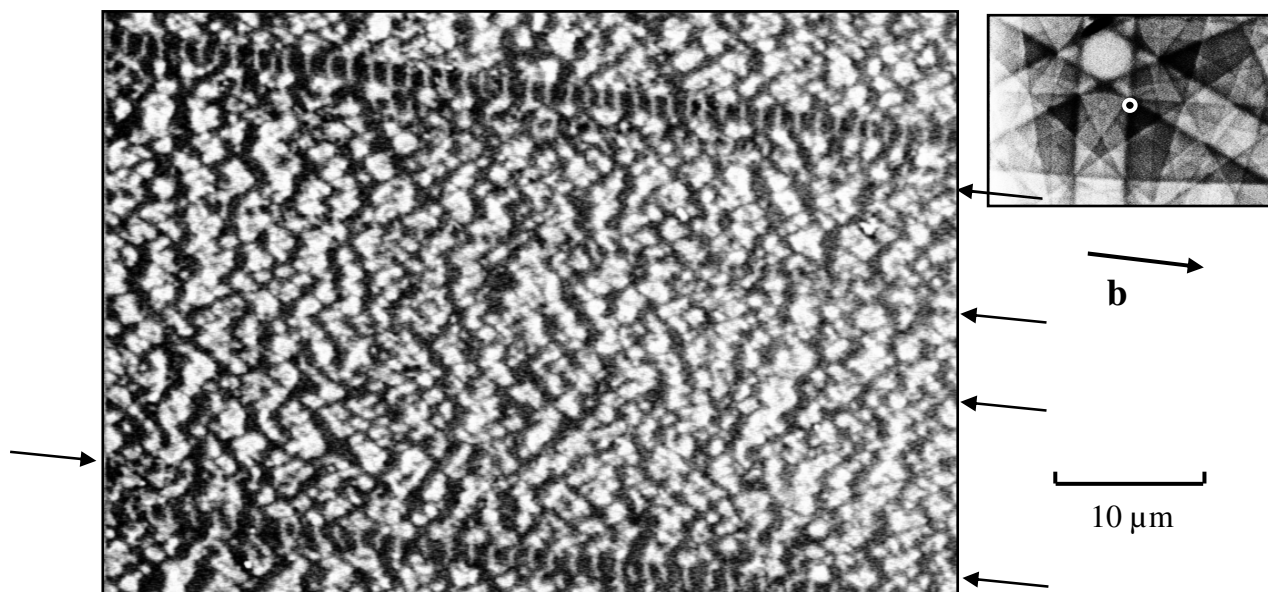
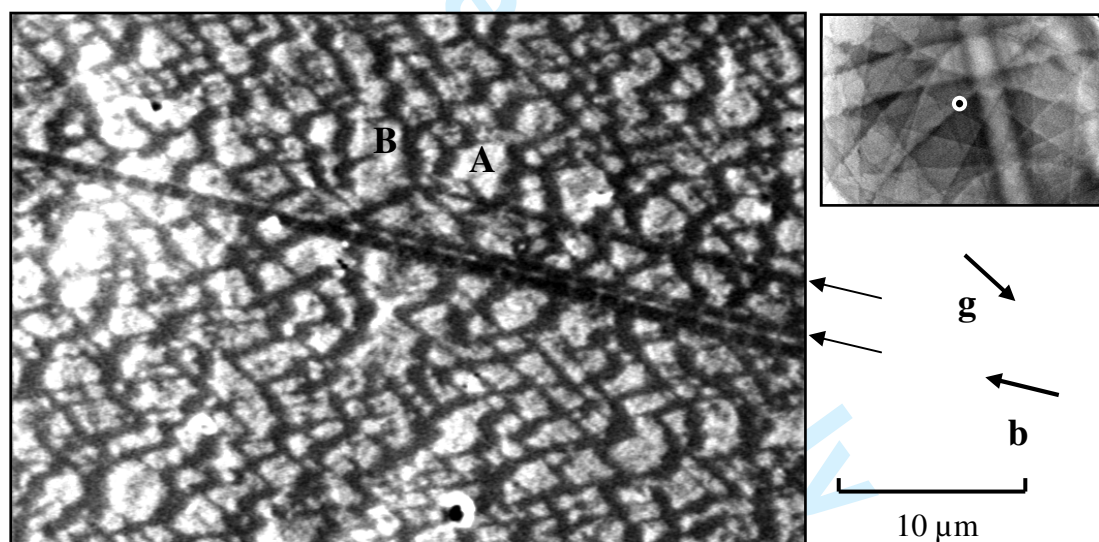


Figure 3: ECCI micrograph obtained from the cross glide face after cycling at a plastic strain amplitude of 2×10^{-3} for 5000 cycles. PSBs have now nucleated within the matrix. Note the inclination of the walls forming the PSBs.



23
24
25
26
27
28
29
30
31
32

Figure 4: ECCI micrograph obtained from the cross glide face after cycling at a plastic strain amplitude of 2×10^{-3} for 40000 cycles. Well-established PSBs span the image and have walls perpendicular to the slip direction. Other thinner PSBs (arrowed) do not span the micrograph.



53
54
55
56
57
58
59
60

Figure 5: ECCI micrograph obtained from the cross glide face after cycling at a plastic strain amplitude of 2×10^{-3} for 180000 cycles. The two arrowed PSBs taper to a point and end within the micrograph.

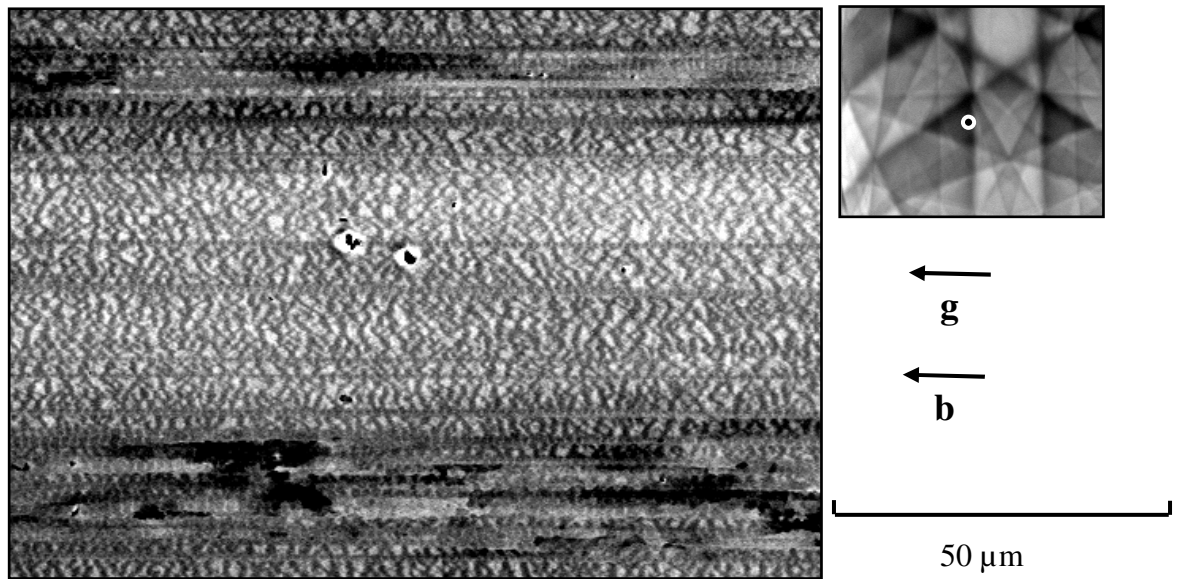


Figure 6: ECCI micrograph obtained from the cross glide face after cycling at a plastic strain amplitude of 10^{-3} for 180000 cycles. Regions at the top and bottom of the micrograph show local misorientations .

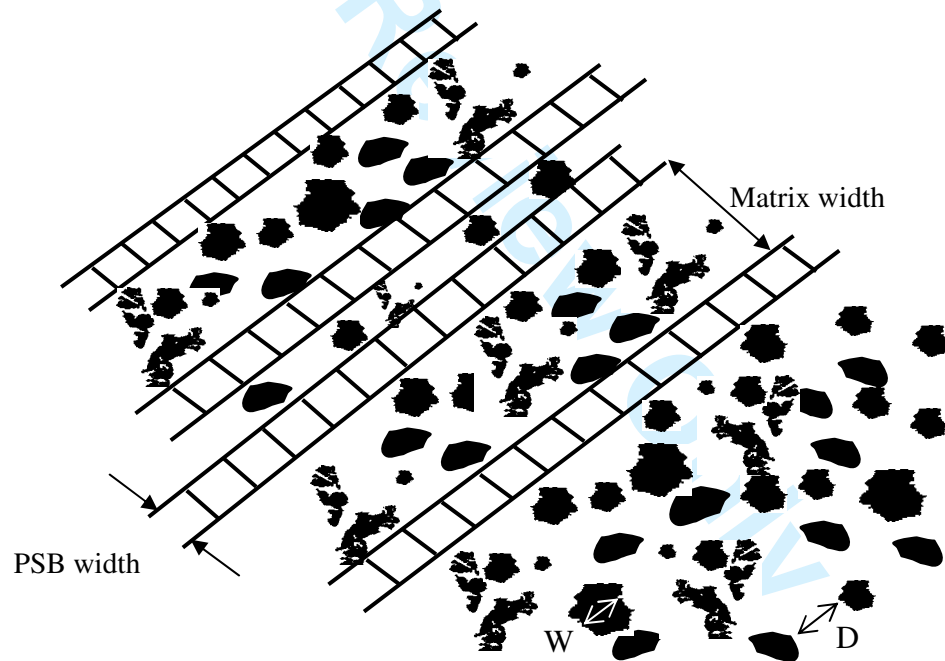


Figure 7: Schematic diagram showing the parameters used to describe the matrix and PSB microstructures.

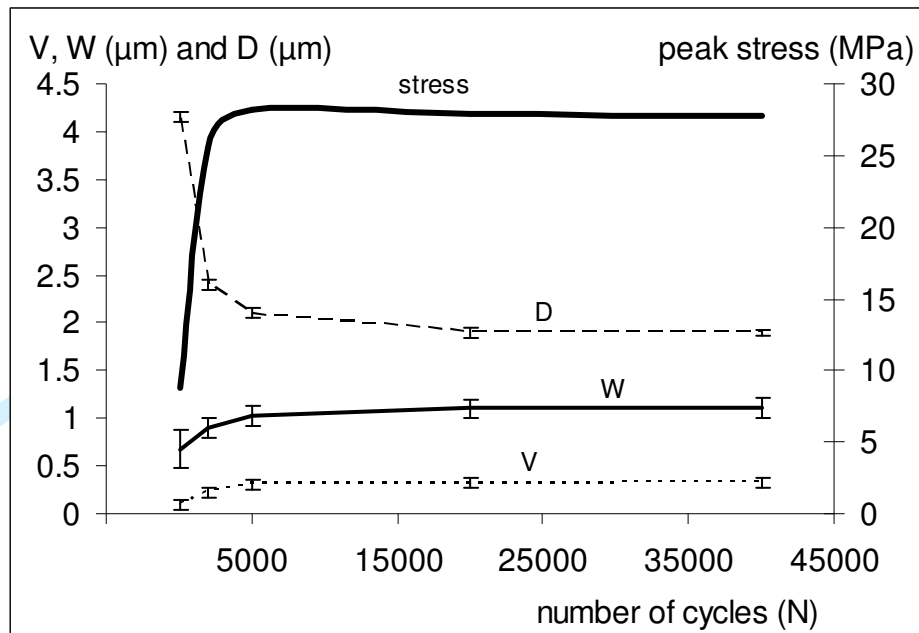


Figure 8: Evolution of vein volume fraction within matrix (V), vein width (W) and channel width D with number of applied fatigue cycles at a plastic shear strain amplitude of 2×10^{-3} .

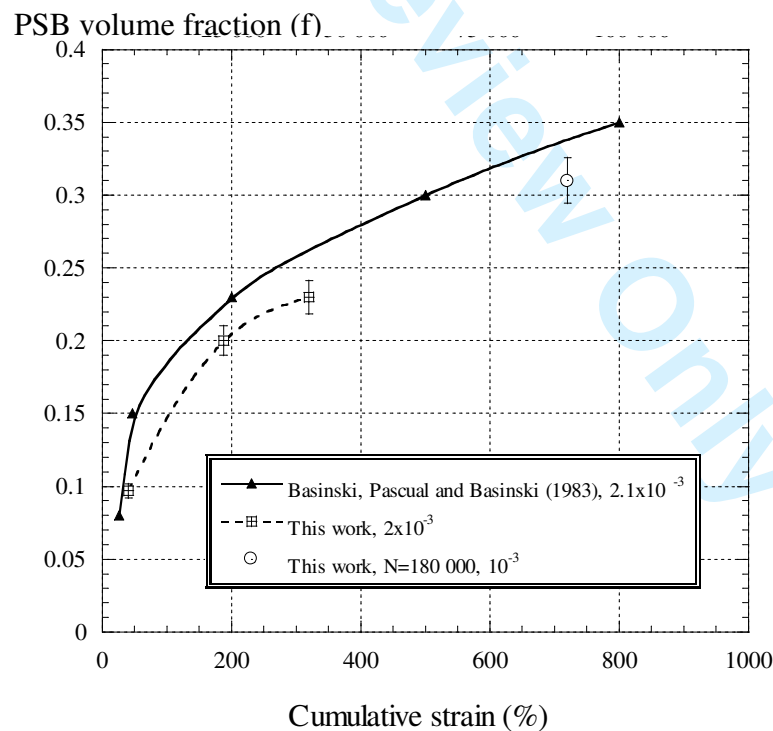


Figure 9: Increase in PSB volume fraction with cumulative strain.

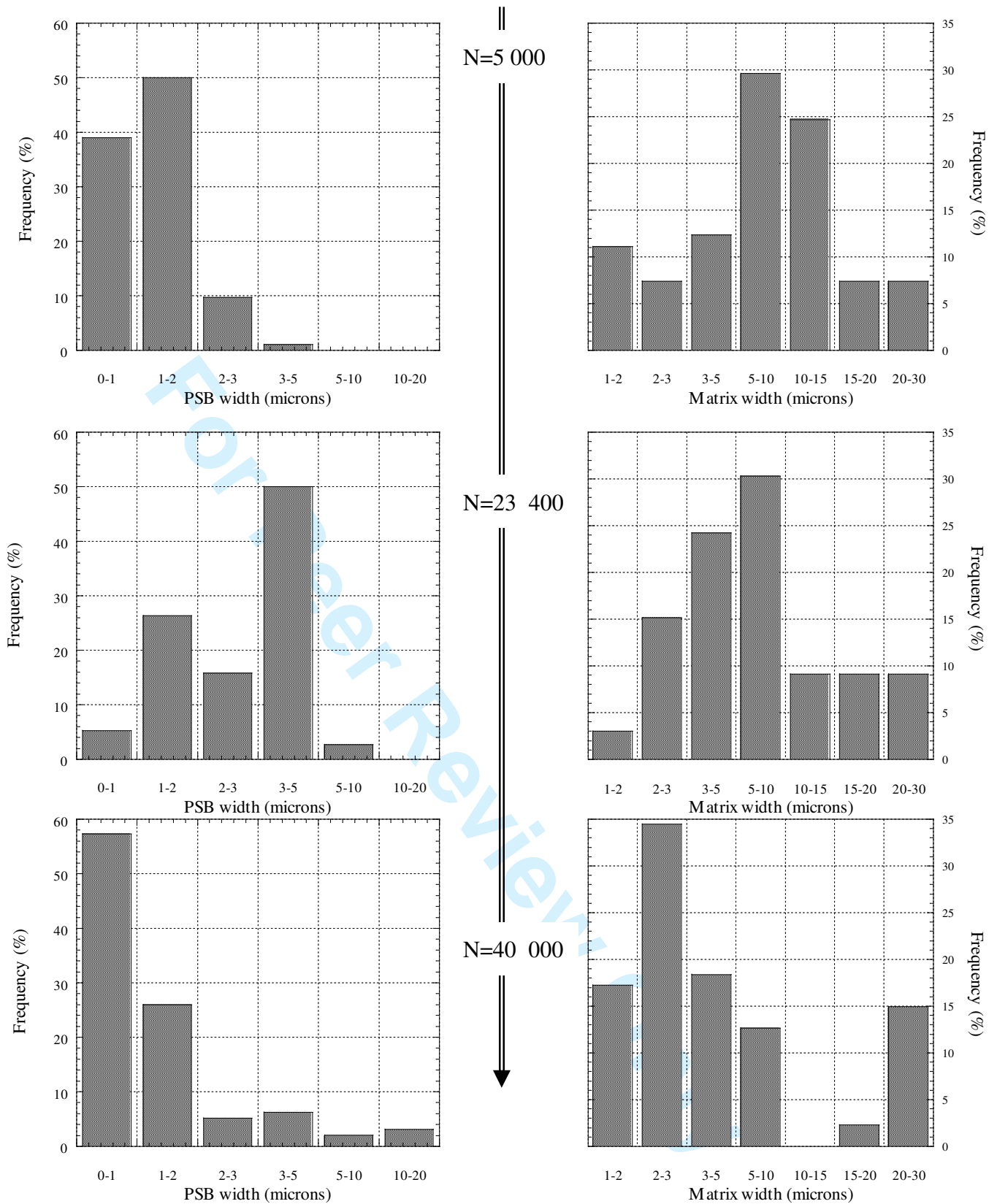


Figure 10: Histograms showing distributions of PSB widths and matrix region widths measured from ECCI micrographs taken of the cross glide face of a sample after fatigue for differing numbers of cycles at a strain amplitude of 2×10^{-3} .

1
2
3
4
5
6
7
8
9
10
11
12
13
14
15
16
17
18
19
20
21
22
23
24
25
26
27
28
29
30
31
32
33
34
35
36
37
38
39
40
41
42
43
44
45
46
47
48
49
50
51
52
53
54
55
56
57
58
59
60

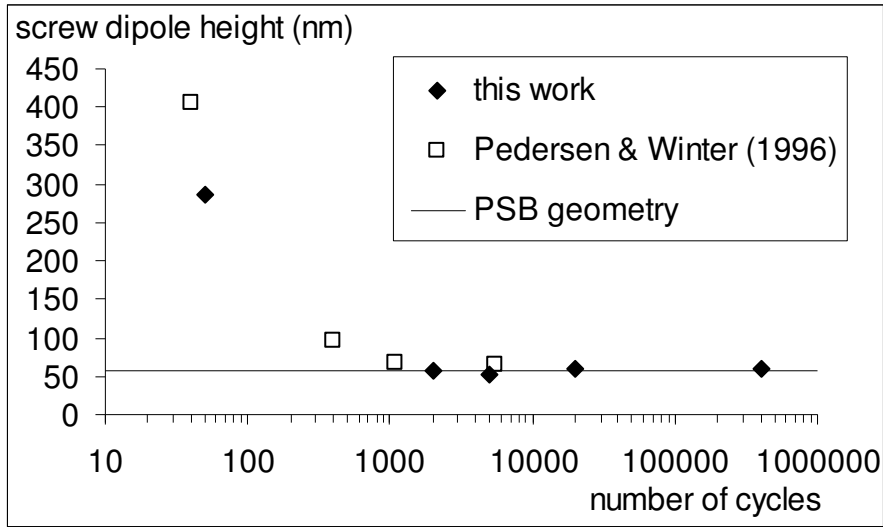


Figure 11: Decrease in calculated height of screw dipoles within matrix channels that are just stable against separation by applied peak stress.